ELSEVIER

Journal of Alloys and Compounds 224 (1995) 330–341

Journal of ALLOYS AND COMPOUNDS

A geometric analysis of solubility ranges in Laves phases

D.J. Thoma [a], J.H. Perepezko [b]

[a] *Los Alamos National Laboratory, Materials Science & Technology Division, Los Alamos, NM 87545, USA*

[b] *University of Wisconsin, Department of Materials Science and Engineering, Madison, WI 53706, USA*

Received 7 October 1994; in final form 18 January 1995

Abstract

Laves phases nominally occur at the AB_2 stoichiometry but can exhibit a range of solubility involving non-stoichiometric compositions in binary alloys. The solubility trends in the reported binary C14, C15 and C36 structures have been analyzed in terms of the atom size requirements that are known to stabilize the Laves phases. For example, Laves phases exist at metallic diameter ratios (D_A/D_B) between ~1.05 and 1.68 with the ideal diameter ratio existing at ~1.225. Although less than 25% of the Laves phases within the D_A/D_B ratios of 1.05–1.68 have defined ranges of homogeneity, the frequency of the number of intermetallic phases exhibiting any solubility range is increased by a factor of approximately two to three within specific D_A/D_B ratios of 1.12–1.26 (C14 and C36 phases) and 1.1–1.35 (C15 phases). The upper and lower bounds for the C15 structures can be physically defined as the limits at which the A–B atom distance contractions are greater than the A–A atom distance and B–B atom distance contractions, respectively. For all three main polytypes the occurrence of solubility corresponds to a lattice-adjusted contraction between 0–15%. The contraction size rule is a geometric argument based upon the contraction of the atoms forming the intermetallic structure and appears to be an important relationship in describing ranges of homogeneity in Laves phases. The relationships developed are applied to interpret potential defect mechanisms and alloying behavior in binary and ternary Laves phases. In addition, extended ternary solubility ranges normal to a pseudobinary direction can be predicted with suitable solute additions having a metallic diameter between that of the A and B atoms.

Keywords: Solubility ranges; Geometric factors; Homogeneity; Laves phases

1. Introduction

1.1. Occurrence and stability of Laves phases

Among the intermetallic phases, the most abundant structural types are the Laves phases (C14, C36, and C15) [1]. The ordered hexagonal C14 Laves phase develops in approximately 131 defined binary phases and 263 defined ternary phases. Similarly, the ordered face-centered cubic C15 Laves phase forms in approximately 219 binary and 272 ternary phases, while 17 binary and 14 ternary phases exist with the ordered hexagonal C36 phase structure [2]. Therefore, considering individual polytypes, over 900 binary and ternary Laves phases have been defined, including over 360 binary Laves phases. The abundance of Laves phase structures has been attributed to geometric principles for the ordered arrangement of atoms on lattice sites [1]. For example, intermetallic phases have the tendency to form with a close packing of atoms, high atomic symmetry, and a metallic nature of bonding (i.e. homogeneous bonding), and Laves phases satisfy the geometric conditions more efficiently than other intermetallic phase structure types [1].

All Laves crystal structure types can be constructed from six four-layer fundamental stacking schemes involving close-packed planes in the close-packed direction of the structure [3]. Geometrically, the structures are slight modifications of each other, with the only difference between Laves polytypes being the periodicity of the stacking schemes (similar to disordered fcc and hcp crystal structures). The space filling and coordination are unchanged between the structures [4], and the packing efficiency is 0.72. The crystal structure and the schematic diagram of the (110) plane in the C15 structure given in Fig. 1 illustrates the position of the A and B atoms in a Laves phase [5]. With spherical atoms in a perfect crystal, the atoms in the AB_2 Laves phases exhibits the ideal diameter ratio $d_A/d_B = \sqrt{3}/\sqrt{2} \approx 1.225$, where d is the diameter of the metal atom at the stoichiometric composition of the intermetallic phase.

SSDI 0925-8388(95)01557-4

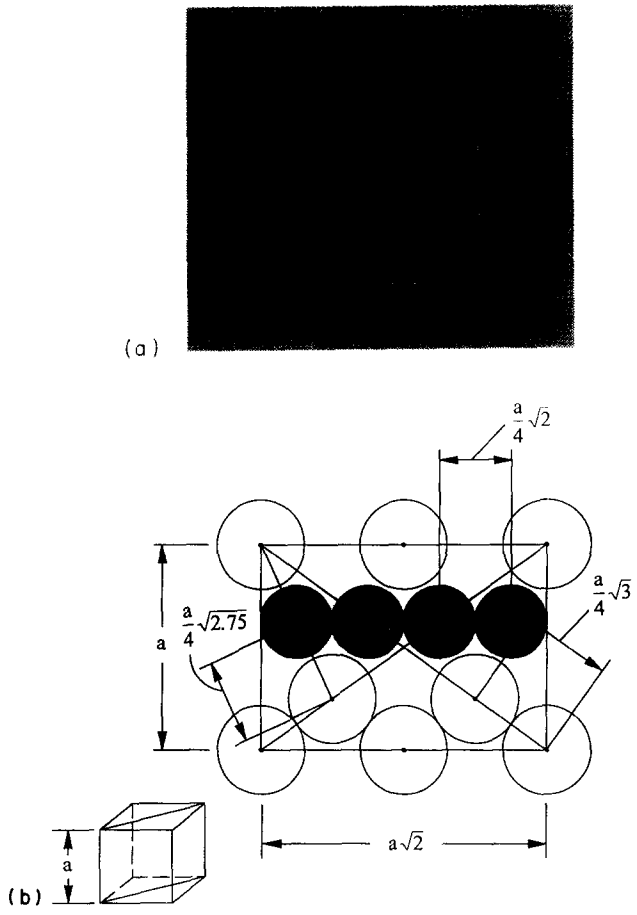

Fig. 1. (a) Schematic diagram of the C15 prototype structure ($MgCu_2$). The A atoms are dark and the B atoms are light. (b) Schematic diagram of the (110) plane in the C15 crystal structure illustrating the distances of the A atoms (open large circles) and B atoms (hatched small circles).

Since Laves phases are predominantly metallic in bonding nature and largely described by geometric space-filling principles, the metallic atom diameter (with a coordination number of 12), D, of the atoms forming the phase has been used often to evaluate the relevance of atomic size factors on the occurrence and relative stability of the Laves phases [1,6,7]. For example, the Laves phases occur between the metallic diameter ratios (D_A/D_B) of ~1.05 and 1.68 [6]. An atom with a metallic diameter, D, will have a different diameter, d, in the Laves phase. The atom size difference between the metallic and intermetallic phases ($D-d$) yields an apparent contraction (positive value) or expansion (negative value) of an atom within the Laves phase. The atoms forming the phase tend to adjust in size to accommodate the ideal space filling ($d_A/d_B \approx 1.225$) in the ordered Laves phase lattice [6], and as a result, the occurrence of the Laves phases is more broadly related to the ability of the A and B atoms to expand or contract so that the ideal ratio is approached. In fact, space-filling models expressed in terms of the compression of A and B atoms and their respective atomic distances (i.e. A–B, A–A, and B–B) have proven to be effective in evaluating the size and volume changes that occur when atoms form a Laves phase [8,9]. The size and volume changes that occur upon Laves phase formation can be further quantified by analyzing specific element groups in the periodic table (e.g. rare earth elements, alkali metals, etc.), and as a result, the position of the atoms in the periodic table has an influence on the occurrence of Laves phases [7,9,10].

The relative stability of the individual Laves phase polytypes (i.e. C14 vs. C15 vs. C36) also is related to the atomic size differences of the atoms forming the phase [6]. The hexagonal polytypes are more abundant where the atom contractions are minimal (i.e. D_A/D_B closer to 1.225), and the C15 polytypes are more frequent with atom size ratios above 1.225. However, distinct trends in the stabilization of the polytypes occur with changing electron concentrations. In fact, a recent study [11] has pointed out that the effectiveness of a geometrical interpretation on the relative stability between Laves phase polytypes (and other structures) is questionable in terms of being a convenient methodology. Alternatively, the study proposes that the analysis of local and global structural effects owing to variations in electron concentration is a more suitable approach to define relative stability. Similar observations have been documented in the literature. For example, in Mg-based Laves phases, the C15 phase is stabilized at electron concentrations (e/a) below 1.8, and the C14 phase is stabilized at higher electron concentrations [12]. In transition-element Laves phases, the C15 phase has been shown to become stable at very large electron concentrations ($e/a > 2.3$) [13] and the C14 phase is stabilized at very low electron concentrations ($e/a < 0.73$) [14]. One of the most interesting effects of electron concentration on stability is found with some AB_2 Laves phases where B = Ni or Co [15]. Many A elements (A = Ti, V, Nb, Ta, Mo, W) do not form a Laves phase with nickel and cobalt, even though the D_A/D_B ratios are favorable for Laves phase formation. However, by substituting silicon on the B lattice sites, ternary C14 compounds can be produced. This phenomenon has been attributed to the binary phases having electron concentrations which are too large. Ternary silicon additions apparently decrease the effective electron concentration, stabilizing a C14 phase [15].

Although Laves phases have been described in terms of geometric principles [1], the relative stability of the respective polytypes are certainly functions of electronic factors as well. Moreover, other factors have been related to the development of Laves phases. As examples, the heats of formation of Laves phases have been correlated to D_A/D_B ratios [16]; electronegativity differences have been used to standardize and fit atom contractions as a function of D_A/D_B ratios [17]; and the crystal structure relationship between the unalloyed

atoms and alloyed phases have been proposed to affect the energetics of Laves phase formation [17]. However, these factors are typically correlated to geometric size ratios, stressing the usefulness of geometric requirements for the interpretation of Laves phase behavior, particularly in the general abundance of the intermetallic phase.

1.2. Solubility in Laves phases

Although the occurrence and relative stabilities of Laves phases have been documented, little information is available on the Laves phase field width and its correlation to the lattice structure in binary phases. The extent of solubility ranges can influence the characteristics and applications of intermetallics [18]. Indeed, the role of ternary solubility in Laves phases has demonstrated potential optimizations in the mechanical properties of Laves phases [19–21]. Owing to the specific arrangement of atoms, deformation involving simple planar slip is unlikely and a "synchroshear" or "zonal-slip" mechanism involving cooperative movement between planes of atoms may be required and can limit the ductility of these materials [19,20]. However, solubility additions on A and/or B lattice sites in the AB_2 Laves phase may be operative in permitting enhanced deformability [21,22]. Moreover, a monolithic intermetallic with some phase field width is more readily processed as compared with a stoichiometric phase. In the following analysis the solubility behavior in Laves phases is explored as a function of the geometric requirements (i.e. atom sizes and atom contractions) in the lattice to identify trends that could provide insight into defining the range of homogeneity and possible defect structures. Although other criteria may influence solubility ranges in Laves phases, the abundance of Laves phases have been described in terms of geometric principles of space filling. Therefore, the geometric space filling requirements of a spherical atom (i.e., geometric factors) involved in the formation of the Laves phases should provide distinct guidelines in judging the extent of solubility.

2. Analysis

Consistent with the geometric analyses of other studies on the stability and occurrence of Laves phases, the metallic atom diameters with a coordination number of 12 [23] are used to evaluate trends in the phase field width of binary Laves phases. The phase field width (i.e. solubility or homogeneity range) is defined to be the maximum total range of solubility (including both sides of stoichiometry) occurring in the Laves phase at any given temperature in the equilibrium diagram. The most recent compilation of binary phase diagrams [24] permitted determination of the currently known solubility ranges in the respective phases. The solubility values were examined as a function of the elemental atomic diameter ratios as well as the contraction of the lattices as determined from the lattice parameters [25]. For the 360 known binary Laves phases, only 25% of the Laves phases have any defined solubility, and less than 20% had a solubility range greater than 2 at.%. For the intent of this study, solubility will be defined as any measurable range of homogeneity (at any temperature) observed in the Laves phase.

2.1. C14 phases

Of the 131 known binary C14 phases, only ~22% of the phases have any known range of solubility. The solubilities of the C14 phases are plotted vs. the atomic diameter ratio in Fig. 2. A clear trend is indicated in the figure, with most examples of solubility occurring in phases that have diameter ratios below ~1.26. Above $D_A/D_B = 1.29$ only one phase out of 35 has any reported solubility, and that phase, $GdMn_2$, contains a lanthanide metal and has an uncertain solubility of 1 at.% [24]. Lanthanide metals are commonly observed to exhibit unique properties due to their electronic configuration in the electron orbitals, particularly the f orbitals. Indeed, the lanthanide contraction, which causes atypical trends in the atomic radii of lanthanide metals in the periodic table, is but one characteristic of these

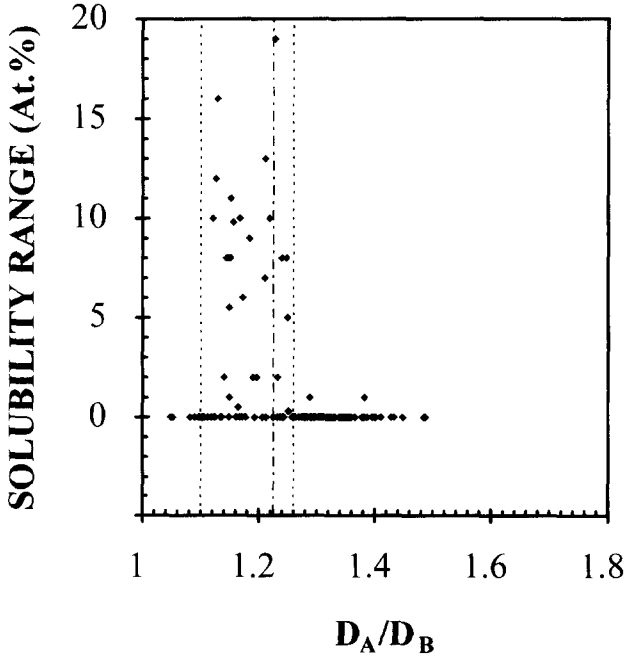

Fig. 2. Plot of the atomic solubility range as a function of the metallic atom diameter ratio in the C14 crystal structures. The middle dashed line is the ideal diameter ratio of ~1.225. The upper and lower dashed diameter ratio bounds indicate the approximate values within which a solubility range is observed.

metals. In fact, it has been proposed that the lanthanide metals can contract to a rather large extent in Laves phases [7].

Between $D_A/D_B = 1.12$ and 1.26, ~53% of the phases exhibit solubility. Clearly, the occurrence of solubility is enhanced as the atoms are closer in size and near the ideal diameter ratio of 1.225, and the observed trend in the diameter ratios is consistent with the required conditions of optimized space filling. Apparently, introduction of constitutional defects on lattice sites generally is more probable within the diameter ratios of 1.12 and 1.26 for the C14 Laves structure.

2.2. C36 phases

As observed with the C14 Laves phase, the less common C36 Laves phase does not typically exhibit solubility above an atomic diameter ratio of 1.26 (Fig. 3). Below $D_A/D_B \approx 1.26$ and above $D_A/D_B \approx 1.12$, 77% of the structures exhibit solubility.

In the intermetallic phases with the C36 structure, only two phases, $NbZn_2$ and $MgNi_2$, do not exist as binary polytypes. These two phases are unusual since studies have suggested that the C36 phase is an intermediate structure in the arrangement sequence of atoms from the C14 to C15 structures [1]. Indeed, TEM studies have offered proof of the structural intermediacy of the C36 phase between polytypes in the $TiCr_2$ intermetallic phase [26]. Moreover, the ternary alloying of continuous Laves solutions of MgX_2 phases indicates that the C36 phase is readily destabilized to the C15 or the C14 structures with minimal negative or positive changes, respectively, in electron concentrations [12].

2.3. C15 phases

For the 219 identified binary C15 Laves phases, ~27% have defined solubility. As demonstrated with the hexagonal Laves phases, solubility clearly increases as the atomic diameter ratios decrease (Fig. 4), and 44% of the phases exhibit solubility between the lower and upper D_A/D_B ratio bounds of 1.1 and 1.35. Above $D_A/D_B = 1.35$, 8 out of 80 phases exhibit solubility (albeit uncertain in many cases), and 7 of these 8 phases contain metals from the lanthanide series. Moreover, above $D_A/D_B = 1.30$, over half of the 26 phases with a range of homogeneity exhibit significant solubility only on the B-rich side of the AB_2 stoichiometric phase. In other words, the lattice appears to be able to accommodate the smaller B atoms on the large A sites, but not vice versa. Below the atomic diameter ratio of 1.35 and above $D_A/D_B = 1.1$, 52 of the 123 phases exhibit solubility, and therefore over 85% of the phases with solubility have diameter ratios within this range.

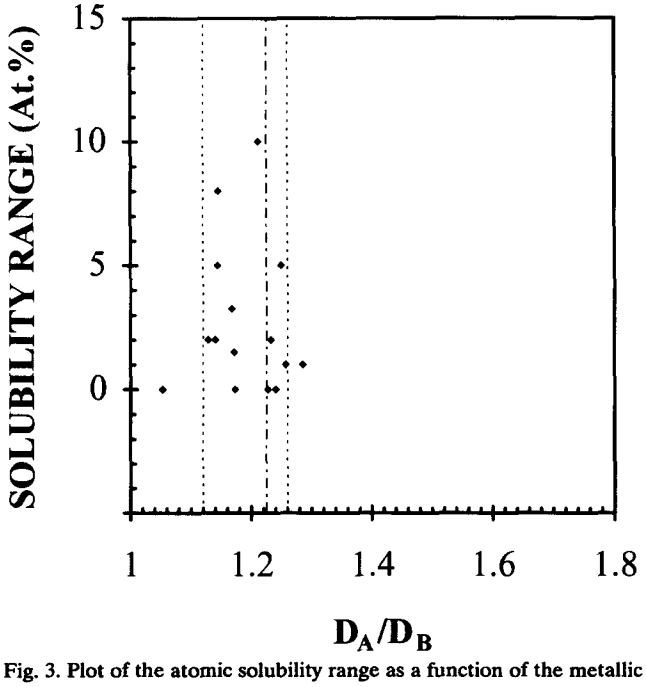

Fig. 3. Plot of the atomic solubility range as a function of the metallic atom diameter ratio in the C36 crystal structures. The middle dashed line is the ideal diameter ratio of ~1.225. The upper and lower dashed diameter ratio bounds indicate the approximate values within which a solubility range is observed.

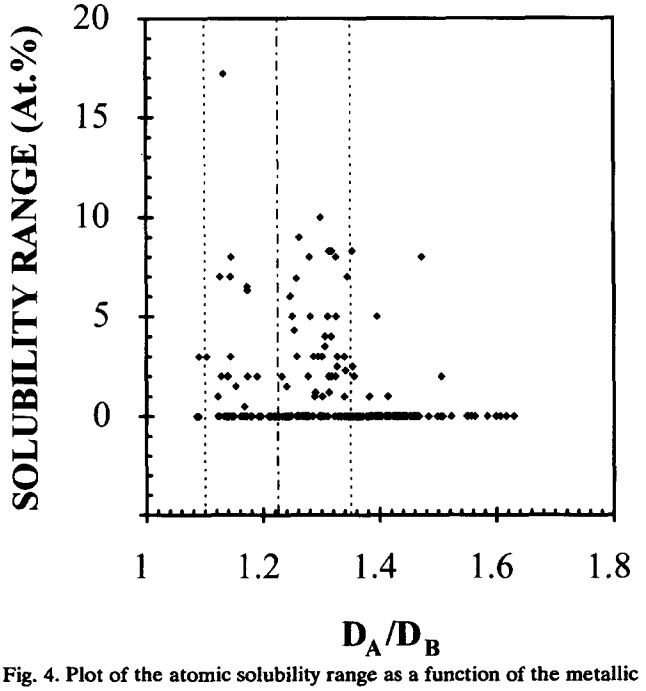

Fig. 4. Plot of the atomic solubility range as a function of the metallic atom diameter ratio in the C15 crystal structures. The middle dashed line is the ideal diameter ratio of ~1.225. The upper and lower dashed diameter ratio bounds indicate the approximate values within which a solubility range is observed.

3. Discussion

3.1. C14 phase

A higher range of solubility is observed for the C14 Laves phases with D_A/D_B ratios between 1.12 and 1.26. The enhanced solubility occurs as the atoms are closer in size to the ideal ratio of 1.225. Therefore, the degree of atom contraction from the metallic diameters to the diameters of the atoms in the phase must influence the occurrence of solubility.

The C14 crystal structure is illustrated in Fig. 5, and the different atom distances are labeled in this figure and defined in the Appendix. With the bond distances defined, the average intermetallic atom size differences

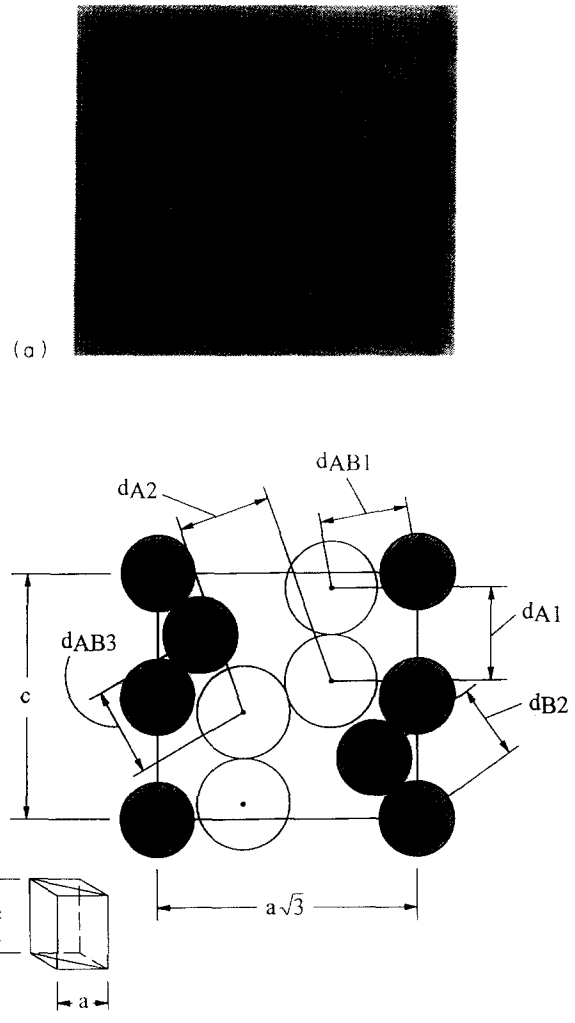

Fig. 5. (a) Schematic diagram of the basic rhombic unit in the hexagonal C14 crystal structure. The A atoms are dark and the B atoms are light. (b) Schematic diagram of a (110) plane of the rhombic unit illustrating the atom distance of the A atoms (open large circles) and B atoms (hatched small circles). The atom distances not shown are: d_{B1}, the distance between the triangularly coordinated B atoms in (a); and d_{AB1}, the distance between the labeled A and B atoms in (a).

with respect to the metallic diameters can be presented in a fashion similar to that shown by Laves [1], only exclusively for the C14 phase (Fig. 6). The average A contraction (i.e. $D_A - d_A$) is demonstrated in Fig. 6(a), whereas Figs. 6(b) and 6(c) illustrate the average B and A–B contractions, respectively. As Laves had noted for the limited number of all Laves phases (C14, C15 and C36) defined at the time of his analysis, the linear regression lines for the A and B contractions intersect at the ideal ratio of ~1.225. The A–B contractions intersect the A and B contractions at D_A/D_B ratios of 1.08 and 1.35, respectively. Although the regression lines were obtained from average contractions of the two A distances, two B distances, and three A–B distances, respectively, the intersections were altered less than 2% with the consideration of the individual distances (i.e. d_{A1} vs. d_{B1}, d_{A1}vs. d_{B2}, d_{A1} vs. d_{AB1}, d_{A2} vs. d_{B1}, etc.).

Since the degree of atom contractions influences the extent of solubility in the C14 Laves phases, the relative contraction (with respect to the metallic atom size) of the A, B, and A–B distances at the stoichiometric composition can be used to interpret the extent of the relative atom size change observed in the phases exhibiting ranges of homogeneity. Figs. 7(a)–7(d) illustrate the average percent contraction of the A atoms, B atoms, A–B distance and an adjusted lattice term plotted respectively vs. solubility. The average percent contraction of the A atoms (i.e. $S_A = 100(D_A - d_A)/D_A$) illustrates that the most extensive solubility occurs in those phases with minimal contractions centered within approximately ±5% of 0% contraction (Fig. 7(a)). The solubility range of the C14 phases with respect to the average percent contractions of the B atoms (i.e. $S_B = 100(D_B - d_B)/D_B$) demonstrates a trend towards solubility in phases with contractions between −3% and 3% (Fig. 7(b)). Solubility as a function of the A–B contractions (i.e. $S_{AB} = 100[((D_A + D_B)/2) - d_{AB}]/(D_A + D_B)/2)$ reflects a trend in observed ranges of homogeneity in phases with strictly negative A–B contractions (i.e. expansions) between 0% and −6% (Fig. 7(c)). Therefore, C14 phases exhibiting a range of solubility display A and B atom contractions centered narrowly around 0%, with the A contractions being slightly broader. In addition, the solubility ranges are observed with only A–B expansions. As a means to combine and interpret the contractions on a scale related to the unit cell, a lattice-adjusted contraction ($S_{lat} = S_A + 2S_B$ for the AB_2 phase) can be used (Fig. 7(d)). The C14 Laves phases typically have a range of solubility when this lattice contraction is within ~0% to 15%. At this point, a comparison of size factors affecting solubility in the metallic Laves intermetallic phase to metallic solid solutions can be made. Hume–Rothery size factor rules on solubility limits in disordered metallic solid solutions have been defined

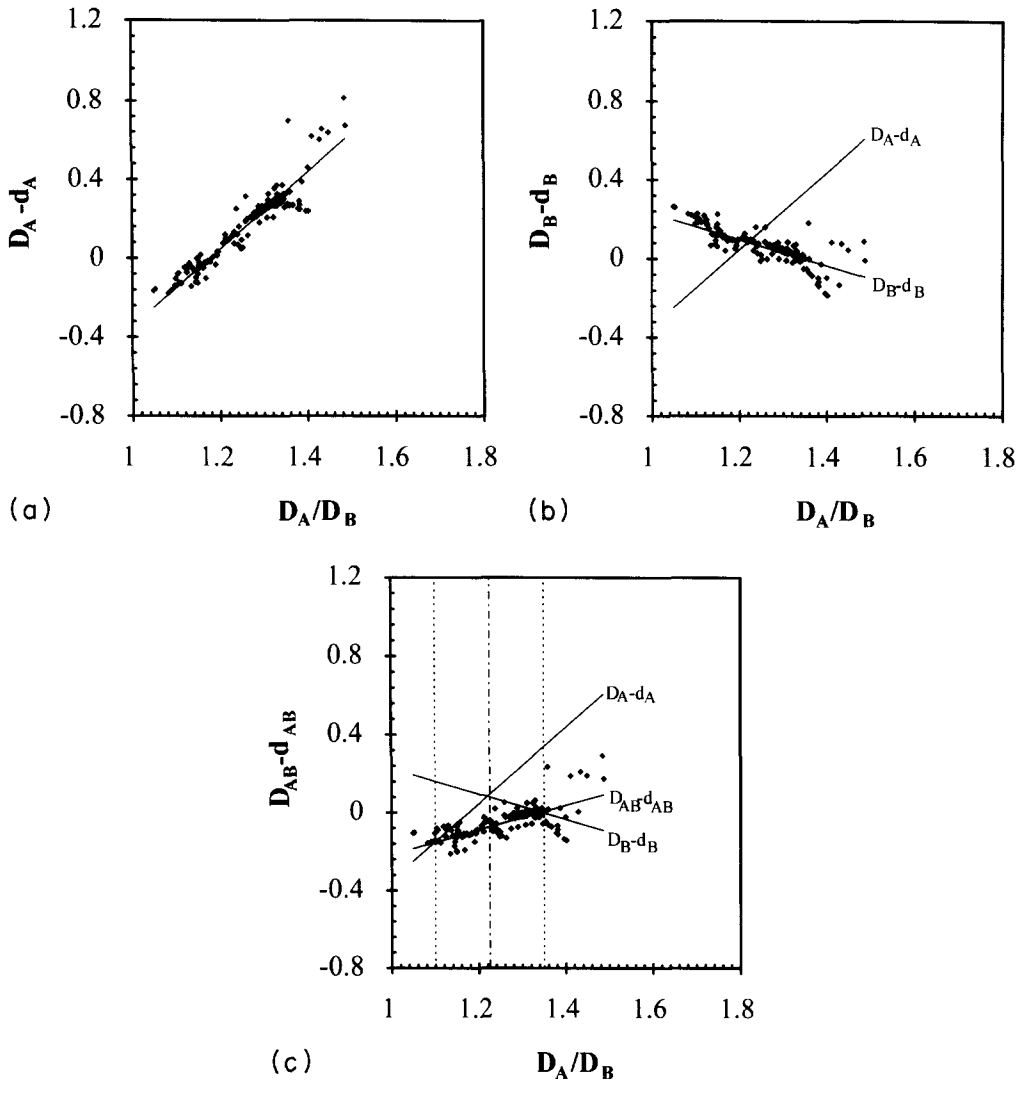

Fig. 6. (a) Contractions of the A–A distances in forming the C14 crystal structures from the metallic elements. (b) Contractions of the B–B distances in forming the C14 crystal structure from the metallic elements. The lines indicate regressions of the A–A distance contractions and B–B distance contractions. (c) Contractions of the A–B distances in forming the C14 crystal structures from the metallic elements. The regression lines (solid) of the A–A distances, B–B distances, and A–B distances are indicated. The vertical dashed lines demark the D_A/D_B ratios at which the contraction regression lines intersect.

for atomic size differences of less than ~15% [27]. The relationships developed in the current analysis for the Laves phase incorporates the difference in atom distances between the metallic and intermetallic solutions and accounts for the atom ratio in the lattice. The Hume–Rothery rule recognizes only the size difference between two metallic atoms. In contrast, the lattice-adjusted contraction size rule reflects a change in atom size in different structures which could originate as a result of electronic structures as well as strain energy.

Owing to the limited number of the other hexagonal Laves phase polytype (C36), a meaningful individual analysis for this phase cannot be performed. However, the C36 phase solubility trends appear to exist within the diameter ratio limits defined for the C14 phase when the data is overlaid onto the C14 plots.

3.2. C15 phase

An increase in solubility was observed for the C15 phases between the D_A/D_B ratios of 1.1 and 1.35. The distances between the atoms in the C15 structure type are labeled in Fig. 1 and defined in the Appendix. The differences in the C15 phase atom separation distance with respect to the elemental diameters are illustrated for the C15 phases in Figs. 8(a)–8(c). The results are essentially identical for the intersection of the C15

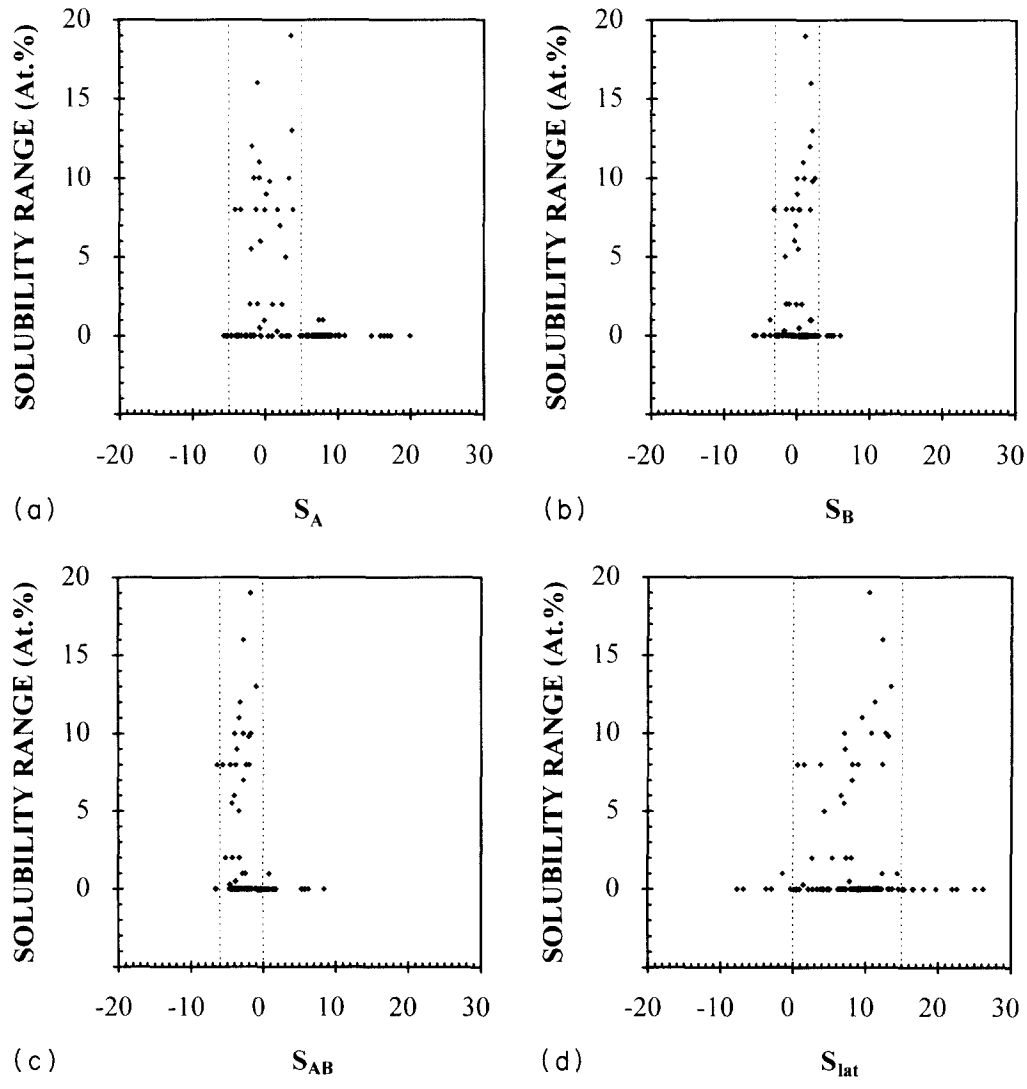

Fig. 7. Solubility ranges of the C14 phases as a function of the relative contractions of the: (a) A–A distance; (b) B–B distance; (c) A–B distance; and (d) overall lattice. The vertical dashed lines indicate the D_A/D_B ratio bounds in which compounds with solubility exist.

Laves phase distance contractions as compared with the C14 Laves phases (Fig. 6), only there are more examples to document the contraction. The linear regression of A and B contraction lines cross at the ideal D_A/D_B ratio of ~ 1.225.

The linear regression lines through the A–B contractions cross the A contraction line at ~ 1.1 and the B contraction line at ~ 1.35. Comparing these results with Fig. 3, the solubility of most of the C15 Laves phases occurs in this range. The few phases with solubility which fall outside of this zone again involve lanthanide elements. Therefore, in the C15 phases, the limits of phases exhibiting solubility occur at the intersection of the A–B contractions with A–A and B–B contractions.

The relative contractions of the individual atom sizes and distance in the C15 phases exhibiting a solubility range are broader and behave differently to those for the C14 phases. The relative atom contractions for the C15 phases and the C14 phases are summarized for comparison in Table 1. Enhanced solubility is observed when the C15 phase A atom contractions are centered about 0%, however, the range of observed solubility incorporates a relative A contraction of $\sim 12\%$ to -8% (Fig. 9(a)). This range of A contractions is approximately twice of that found with the C14 phases. Again, C15 phases with a solubility range outside these limits involve lanthanides. The C15 phases with solubility occur with B contractions between 0 and 5% (Fig. 9(b)), whereas the B contractions for the C14 phase were centered around 0% ($\pm 3\%$), and include negative contractions. The C15 phases with solubility generally exist with 3% to -7% contractions of the A–B distance (Fig. 9(c)), whereas the C14 phase A–B distance contractions gen-

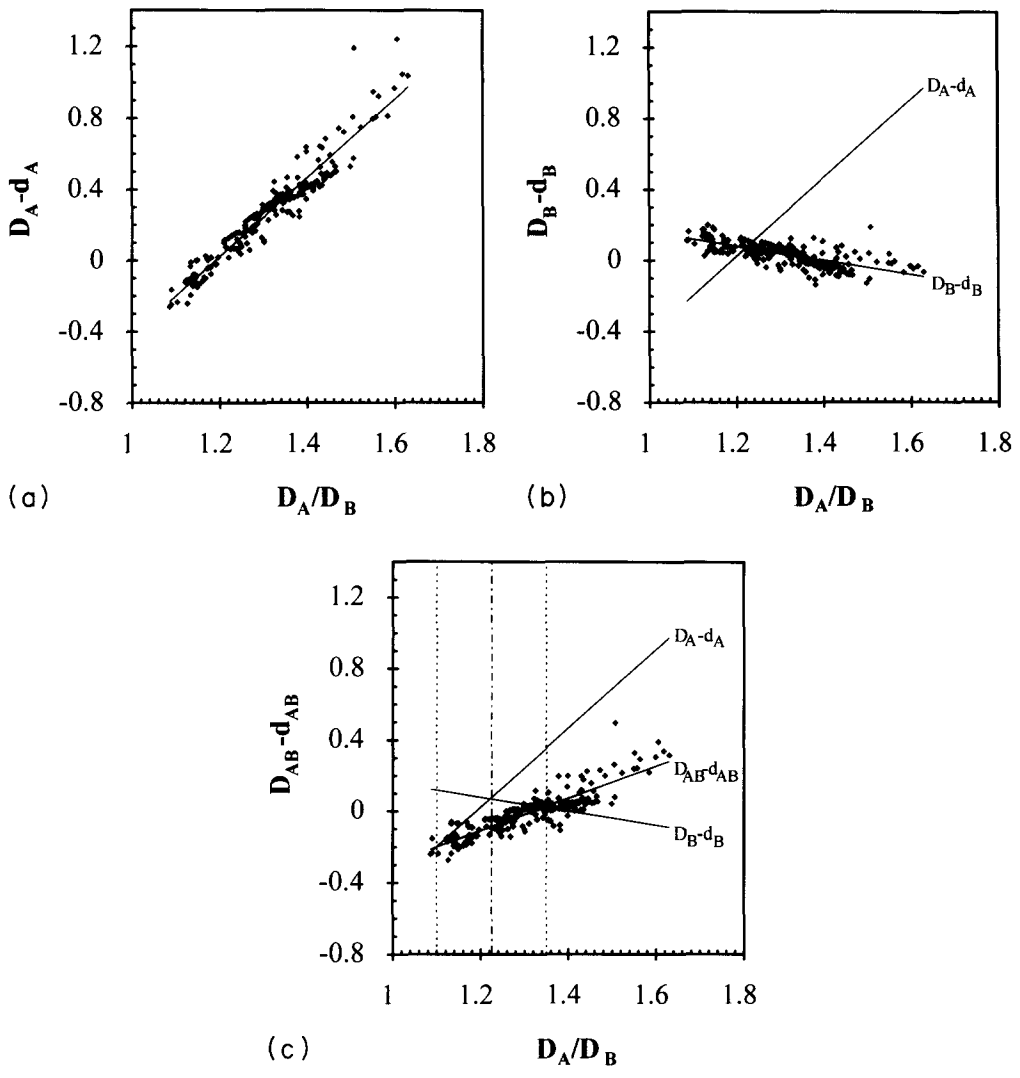

Fig. 8. (a) Contractions of the A–A distances in forming the C15 crystal structures from the metallic elements. (b) Contractions of the B–B distances in forming the C15 crystal structure from the metallic elements. The lines indicate regressions of the A–A distance contractions and B–B distance contractions. (c) Contractions of the A–B distances in forming the C15 crystal structures from the metallic elements. The regression lines (solid) of the A–A distances, B–B distances, and A–B distances are indicated. The vertical dashed lines demark the D_A/D_B ratios at which the contraction regression lines intersect.

Table 1
Ranges of the relative atomic distance contraction for the C15 and C14 Laves phases exhibiting solubility

Crystal structure	S_A	S_B	S_{AB}	S_{lat}
C14	−5% to 5%	−3% to 3%	−6% to 0%	0% to 15%
C15	−8% to 12%	0% to 5%	−7% to 3%	0% to 15%

$S_A = 100(D_A - d_A)/D_A$; $S_B = 100(D_B - d_B)/D_B$; $S_{AB} = 100(D_{AB} - d_{AB})/D_{AB}$; $S_{lat} = S_A + 2S_B$.

erally were not positive (0% to −6%). Therefore, the C15 Laves phases with observed ranges of solubility tend to exhibit greater atom distance contractions than the C14 phases with defined solubility ranges. The extents of negative and positive contractions also are different. However, the C15 Laves phases with observed ranges of solubility represent an adjusted lattice contraction range of 0–15% for binary Laves phase structures (Fig. 9(d)). Despite the differences in the relative atom size contractions between the C14 and C15 Laves phases, the polytypes can be normalized to exhibit solubility within identical size rules (S_{lat}) of 0–15%.

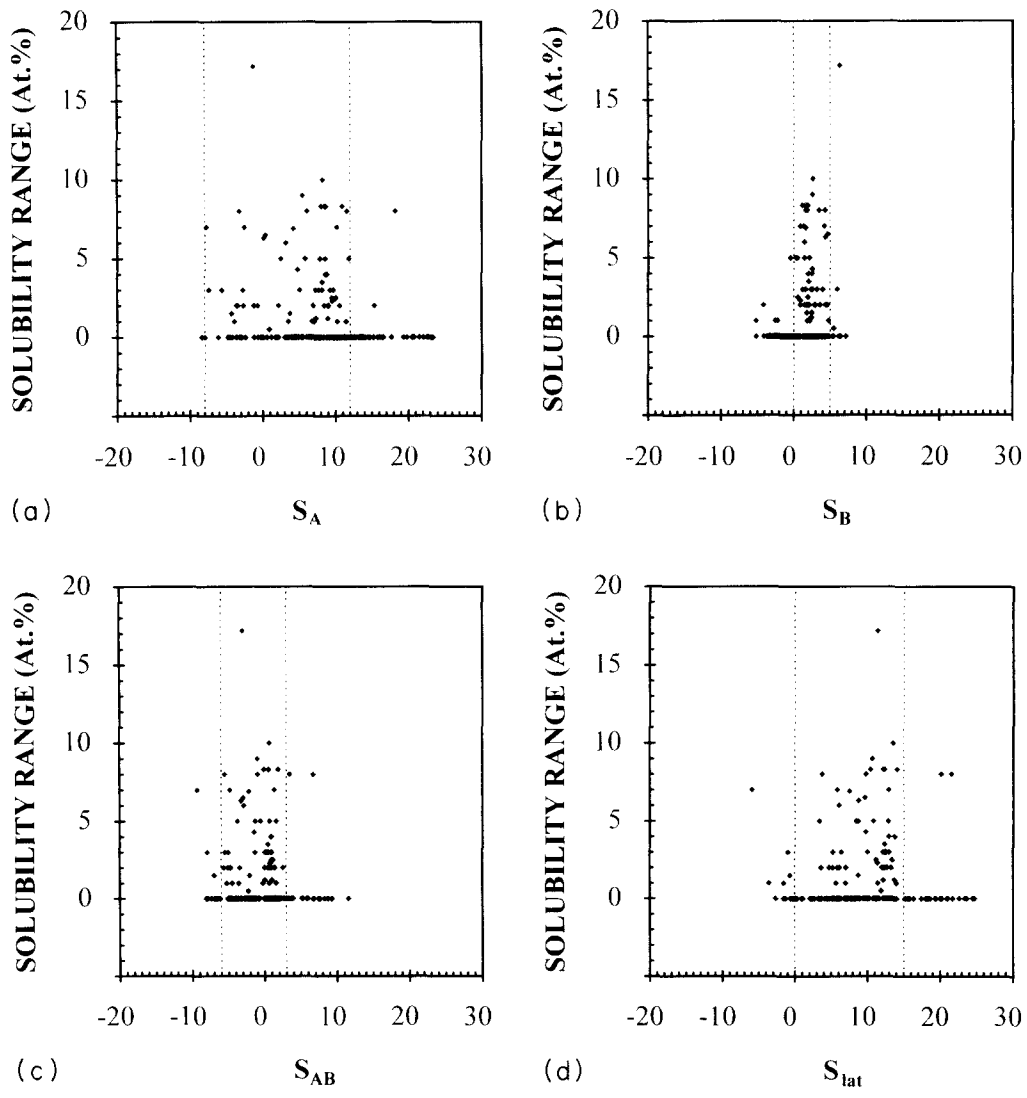

Fig. 9. Solubility ranges of the C15 phases as a function of the relative contractions of the: (a) A–A distance; (b) B–B distance; (c) A–B distance; and (d) overall lattice. The vertical dashed lines indicate the D_A/D_B ratio bounds in which compounds with solubility exist.

3.3. Consequences of atom size limits on solubility ranges

3.3.1. Defect behavior

In systems with solubility, an analysis of solubility range vs. D_A/D_B reveals a direct correlation between the atomic size and the phase field width. Generally, solubility occurs between diameter ratios of 1.12 and 1.26 (C14 and C36), and 1.1 and 1.35 (C15). Within this range, the atoms are close enough in size to apparently accommodate constitutional defects. With D_A/D_B ratios greater than the ideal ratio, solubility on the B-rich side of stoichiometry is more pronounced and can be explained in terms of geometric requirements. For example, substitution of the larger A atoms on the B sites should be more difficult in the geometrically restrictive lattice as compared with the substitution of the smaller B atoms on A sites. Therefore, above the ideal D_A/D_B ratios the geometric substitution only can occur with the smaller B atoms filling the A sites. Accordingly, over half of the 26 C15 phases exhibiting a solubility range with D_A/D_B ratios over 1.3 have solubility only on the B-rich side of the AB_2 stoichiometry.

Based upon geometric space-filling arguments, antisite substitution appears to be a likely defect mechanism for Laves phases on the B-rich side of stoichiometry. Analyses of the presence of substitutional B atoms on A lattice sites has been suggested in the C15 phases, $ZrFe_2$ ($D_A/D_B=1.26$) [28] and $NbCo_2$ ($D_A/D_B=1.17$) [29] and $NbCr_2$ ($D_A/D_B=1.15$) [30]. Moreover, the metallic diameter ratios could influence the extent of solubility in metastable solubility extensions during rapid solidification processing. For example, YAl_2 ($D_A/D_B=1.27$) exists as a stoichiometric phase under equilibrium conditions, but with rapid solidification processing, an extended metastable range of solubility has been promoted on the Al-rich side of stoichiometry

[31]. Limited extended solubility could also be obtained on the Y-rich side of stoichiometry. The defect mechanism was suggested to consist of anti-site substitution of Al on Y lattice sites on the Al-rich side of stoichiometry.

On the A-rich side of stoichiometry, the specific defect mechanism is not as well defined. Based upon the lattice parameter behavior as a function of composition in the C15 $NbCr_2$ phase ($D_A/D_B=1.15$), the occurrence of constitutional defects involving vacancies has been speculated on the Nb-rich side of stoichiometry [30]. Similarly, for the C15 YAl_2 phase ($D_A/D_B=1.27$) the occurrence of Al vacancies was suggested to occur as a constitutional defect on the Y-rich side of stoichiometry [31]. Because of the geometric limitation in size for the A atoms existing as anti-site substitutions on B atom sites, B vacancies could be an appropriate constitutional defect. However, the defect mechanisms have not been defined specifically in the $NbCr_2$ and YAl_2 phases, and in fact, the reported C15 phase defect mechanisms on any A-rich side of stoichiometry are limited. One study has experimentally attempted to define the defect mechanism on both sides of stoichiometry, and anti-site substitution occurring on both sides of stoichiometry for the C15 phase, $ZrCr_2$ ($D_A/D_B=1.25$), was reported [32]. The size discrepancy of substituting a large Zr atom on a Cr lattice site apparently is accommodated in this intermetallic phase. Similarly, anti-site substitution on both sides of stoichiometry has been proposed for some C14 phases: $TiFe_2$ ($D_A/D_B=1.14$) [28,33] and $NbFe_2$ ($D_A/D_B=1.16$) [34]. $TiFe_2$ and $NbFe_2$ have low diameter ratios, and since the metallic atoms are close in size, anti-site occupancy is physically realistic. Therefore, defect mechanisms on the A-rich side of stoichiometry may be sensitive to the role of atomic sizes in the Laves phase polytypes, but certainly further research is required to more completely identify the appropriate defect mechanisms.

The characterization of defect mechanisms in Laves phases is relevant to many physical properties. For example, the types of constitutional defects are important in the operative diffusion mechanisms in Laves phases [35], and diffusion mechanisms contribute to the high temperature stability and mechanical strength of the material. In addition, the existence of vacancy defects may assist the synchroshear process in Laves phases [36], providing potential ductility to the intermetallic phase.

3.3.2. Alloying behavior

The geometric rules affecting solubility that have been developed in this study apply both to binary and ternary alloying additions. In binary phases, an observed increase in the occurrence of phases that exhibit solubility exists within specific size ratios. However, many of the phases that do not have a defined solubility range may indeed display a range of homogeneity under more careful studies. Many of the phase diagrams utilized in this analysis indicate dotted lines or use limited sources of data to define the phase fields.

For ternary phases, the extension of the solubility trends observed in binary systems can be used to anticipate potential solubility changes owing to ternary element additions. The existing database on ternary Laves phase field extent is limited. Most systematic studies have focused on pseudobinary behavior where the ternary addition (i.e. C) to the AB_2 structure is considered to substitute as $(A,C)B_2$ or $A(B,C)_2$. In this case the usual considerations for promoting extensive solubility (i.e low atomic size mismatch) may be applied to select a suitable solute. The approach is quite successful in phase-field extension except when the ternary solute addition yields a transition between Laves phase structures such as the classic example of $MgNi_2$–$MgCu_2$ [12].

When the extension of the solubility range normal to the pseudobinary direction is considered, the results of the current analysis reveal other factors for solute selection. In order to allow for effective substitution, the relation $D_A>D_C>D_B$ should be obeyed. In this way solute C atoms can substitute for both A and B atoms. This criterion has been demonstrated for $NbCr_2$, where Ti additions nearly double the width of the C15 phase field normal to the $NbCr_2$–$TiCr_2$ section [37]. Even more dramatic is the extension of the C15 HfV_2 phase field from about 1 at.% at 1000 °C to a range ~20 at.% wide with the addition of 20 at.%Nb [38]. For both $NbCr_2$ and HfV_2 the atomic diameter ratio is below 1.225 and the ternary solute atom diameter is between the binary atom diameters.

4. Summary

Less than 25% of binary Laves phases exhibit solubility, but the Laves phases that do exhibit a range of homogeneity can be described with distinct atom size arguments. The probability for increased equilibrium (as well as metastable) solubility is markedly improved as the ratio of elemental metallic atom diameters approaches the ideal ratio of 1.225. This empirical trend for increased solubility is consistent with the geometric restrictions and requirements of space filling in the Laves metallic phases, and in this study, has been interpreted on a quantitative fashion with three main points.

(1) The observation of a solubility range is increased approximately two to three times within specific D_A/D_B ratios of 1.12–1.26 and 1.1–1.35 for the C14 and C15 phases, respectively.

(2) For the C15 phases, the diameter ratio bounds are defined physically by the intersection of linear regression lines for the A–B distance contraction with the A and B atom contractions.

(3) Despite the different diameter ratio ranges, all Laves polytypes exhibit solubility between adjusted lattice contractions of 0–15%. The lattice-adjusted contraction size rule developed in this present work accommodates the geometric consequences of atom size changes upon forming the intermetallic structure.

The geometric arguments affecting solubility defined in this study provide a platform to interpret phase field width and potential defect mechanisms in Laves phases.

Acknowledgments

The support of ARPA (ARO-DAAL-03-90-G-0183) is gratefully acknowledged. In addition, the authors thank Dr. L.A. Jacobson, Dr. F. Chu, Dr. T.E. Mitchell, Prof. D. de Fontaine, Dr. M. Sluiter, and J.C. Foley for their insightful comments and useful discussions.

Appendix

C14 bond distances

The respective A–A, B–B, and A–B distances are not all equidistant unless the axial ratio c/a is exactly $\sqrt{(8/3)}$ [6]. At $c/a=\sqrt{(8/3)}$, d_A/d_B is equal to $\sqrt{(3/2)}$. Following Berry and Raynor [6] for non-ideal axial ratios, two distances can be defined for both the A and B atoms. The A distances (A1 and A2) are

$$d_{A1}=c(1/2-2z)$$

and

$$d_{A2}=[a^2/3+(2cz)^2]^{1/2}$$

where z is a parameter which defines the relative position of A atoms above or below the basal plane. The value of z is dependent upon the specific alloy phase but is very near 1/16 [6]. The B distances (B1 and B2) can be defined as follows:

$$d_{B1}=(1+3x)a$$

and

$$d_{B2}=(3x^2a^2+c^2/16)^{1/2}$$

where x corresponds to the B atom position in the lattice with respect to the a lattice parameter and is approximately $-1/6$ [6]. In addition to the A and B distances, the A–B distances (AB1, AB2, and AB3) can be defined as:

$$d_{AB1}=(a^2/3+c^2z^2)^{1/2}$$

$$d_{AB2}=[a^2(1/3+x+3x^2)+c^2(1/4-z)^2]^{1/2}$$

and

$$d_{AB3}=[3a^2(1/3+x)^2+c^2(z+1/4)^2]^{1/2}$$

C15 bond distances

The distances between the atoms in the C15 structure type are defined as follows:

$$d_A=(a\sqrt{3})/4$$

$$d_B=(a\sqrt{2})/4$$

and

$$d_{AB}=(a\sqrt{11})/8$$

References

[1] F. Laves, *Theory of Alloy Phases,* ASM, Cleveland, OH, 1956, p. 123.
[2] P. Villars and L.D. Calvert (eds.), *Pearson's Handbook of Crystallographic Data for Intermetallic Phases,* 1st edn., ASM, Cleveland, OH, 1985.
[3] Y. Komura, *Acta Crystallogr., 15* (1962) 770.
[4] G.V. Raynor, *The Physical Metallurgy of Magnesium and Its Alloys,* Pergamon Press, New York, NY, 1959, p. 167.
[5] G.E.R. Schulze, *Z. Elektrochem., 45* (1939) 849.
[6] R.L. Berry and G.V. Raynor, *Acta Crystallogr., 6* (1953) 178.
[7] A.E. Dwight, *Trans. ASM, 53* (1961) 479.
[8] W.B. Pearson, *Acta Crystallogr., B24* (1968) 7, 1415.
[9] W.B. Pearson, *Acta Crystallogr., B37* (1981) 1174.
[10] Y. Ohta and D.G. Pettifor, *J. Phys.: Condensed Matter, 2* (1990) 8189.
[11] R. Nesper and G.J. Miller, *J. Alloys Comp., 197* (1993) 109.
[12] F. Laves and H. Witte, *Metallwirtschaft, 15* (1936) 840.
[13] R.P. Elliot and W. Rostoker, *Trans. ASM, 50* (1958) 617.
[14] W.E. Wallace and R.S. Craig, *Phase Stability of Metals and Alloys,* ASM, Cleveland, OH, 1966, p. 255.
[15] D.I. Bardos, K.P. Gupta and P.A. Beck, *Trans. AIME, 221* (1961) 1087.
[16] G.M. Campbell, in H. Blank and R. Linder (eds.), *Plutonium and Other Actinides,* North-Holland, Amsterdam, 1976, p. 95.
[17] A.R. Edwards. *Metall. Trans., 3* (1972) 1365.
[18] Y.A. Chang and J.B. Neumann, *Prog. Solid State Chem., 14* (1982) 221.
[19] J.D. Livingston, E.L. Hall and E.F. Koch, *Mat. Res. Soc. Symp. Proc., 133* (1989) 243.
[20] J.D. Livingston, *Mat. Res. Soc. Symp. Proc., 322* (1994) 395.
[21] J.D. Livingston and E.L. Hall, *J. Mat. Res., 5* (1) (1990) 5.
[22] F. Chu, *Ph.D. Thesis,* University of Pennsylvania, 1993.
[23] W.B. Pearson, *The Crystal Chemistry and Physics of Metals and Alloys,* Wiley, New York, NY, 1972, p. 151.
[24] T.B. Massalski (ed.), *Binary Alloy Phase Diagrams,* 2nd edn., ASM, Materials Park, OH, 1990.
[25] P. Villars and L.C. Calvert (eds.), *Pearson's Handbook of Crystallographic Data for Intermetallic Phases,* 2nd edn., ASM, Materials Park, OH, 1991.
[26] C.W. Allen, *Mat. Res. Soc. Symp. Proc., 39* (1985) 141.
[27] W. Hume-Rothery, G.W. Mabbott and K.M. Channel-Evans, *Phil. Trans. Roy. Soc., A223* (1934) 1.

[28] W. Bruckner, K. Kleinstuck and G.E.R. Schulze, *Phys. Stat. Sol., 23* (1967) 475.
[29] J.K. Pargeter and W. Hume-Rothery, *J. Less-Common Met., 12* (1967) 366.
[30] D.J. Thoma and J.H. Perepezko, *Mater. Sci. Eng., A156* (1992) 97.
[31] J.C. Foley, D.J. Thoma and J.H. Perepezko, *Metall. Mater. Trans. A, 25* (1994) 230.
[32] R.L. Fleischer, *Scr. Metall. Mater., 27* (1992) 799.
[33] W. Bruckner, R. Perthel, K. Kleinstuck and G.E.R. Schulze, *Phys. Stat. Sol., 29* (1968) 211.
[34] A.W. Smith, J.A. Rogers and R.D. Rawlings, *Phys. Stat. Sol., (a) 15* (1973) K119.
[35] H. Mehrer, W. Sprengel and M. Denkinger, in B. Fultz, R.W. Cahn and D. Gupta (eds.), *Diffusion in Ordered Alloys,* TMS, Warrendale, PA, 1993, p. 51.
[36] P.M. Hazzledine, in M.H. Yoo and M. Wuttig (eds.), *Twinning in Advanced Materials,* TMS, Warrendale, PA, 1994, p. 403.
[37] D.J. Thoma and J.H. Perepezko, in J.E. Morral, R.S. Schiffman and S.M. Merchant (eds.), *Experimental Methods of Phase Diagram Determination,* TMS, Warrendale, PA, 1994, p. 45.
[38] F. Chu and D.P. Pope, *Scr. Metall. Mater., 28* (1993) 331.